Magnetization processes in nickel and cobalt electrodeposited nanowires

R. Ferré* and K. Ounadjela
IPCMS, 23 Rue du Loess, F-67037 Strasbourg Cedex, France

J. M. George
Unité Mixte de Physique CNRS/Thomson, F-91404 Orsay, France

L. Piraux and S. Dubois
Département des Sciences des Matériaux et des Procédés, Université Catholique de Louvain, Place Croix du Sud 1, B-1348 Louvain la Neuve, Belgium

(Received 25 March 1997)

We report on the magnetic properties of arrays of submicronic (35 nm-500 nm) Ni and Co wires fabricated by electrodeposition into the cylindrical pores of track-etched polymer membranes. This work reveals intrinsic differences between the magnetization reversal mechanisms taking place in these two systems. For Ni, the crystal anisotropy is small compared to the shape anisotropy and the magnetization lies along the wire axis. In contrast, the strong crystal anisotropy of Co and the orientation of the crystal easy axis (nearly perpendicular to the wire axis), allows for the appearance of a multidomain magnetization configuration, each domain being oriented partially along the normal to the wire axis. Experimental evidence for the existence of this multidomain configuration has been obtained from resistivity and magnetization measurements. Large scale micromagnetic calculations for Co and Ni wires with high aspect ratios corroborate the strong influence of the crystal anisotropy on the overall properties of Co wires and provide an accurate microscopic description of the nucleation fields and the magnetization reversal mechanism for Ni wires. [S0163-1829(97)08045-4]

I. INTRODUCTION

Pioneer studies of the magnetization processes in elongated particles in the light of micromagnetic theory[1] were carried out in the mid-60's on single-crystal bars (whiskers) prepared by evaporation techniques.[2] Early experiments such as those carried out by Luborski and Morelock[3,4] on ensembles of iron whiskers showed a relatively poor general agreement between the measured coercive fields as a function of the radius and theoretical results for the nucleation fields in a cylinder with infinite length (infinite cylinder model). These pioneering experiments also indicated the enormous difficulty to interpret the experimental results obtained for ferromagnetic bars of finite length in terms of simple micromagnetic models such as the infinite cylinder.[5]

Mainly motivated by the technological interest involving the miniaturization of sensors and the continuous increase of the magnetic storage density, techniques for fabrication (such as nanolithography) and characterization (near field microscopy, electronic microscopy, and holography) of magnetic materials have been developed.[6] To date, elaboration methods such as molecular-beam epitaxy or laser ablation followed by nanolithography of ever-increasing resolution, are usually considered to represent the ultimate limit for producing nanoscale magnets. However, well crystallized nanomagnets can also be fabricated using a different method that provides a very interesting quality vs price ratio, and whose key steps are ''template and electrodeposition''.[7] In this method, nanowires of magnetic metals with extremely large aspect ratio (as large as 10^3) are electrochemically synthesized within the voids of a nanoporous material, such as alumite media[8,9] and track-etched polymer membranes.[10] In these previous works, the highly anisotropic magnetic properties of such arrays have been clearly demonstrated. Recently, arrays of magnetic multilayered nanowires exhibiting giant magnetoresistance were also fabricated using this strategy.[11] Using micro-superconducting quantum interference devices (SQUID's) and magnetic force microscopy,[12,13] magnetization reversal studies have been recently performed on single Ni nanowires. Statistical studies of thermally activated magnetization reversal in Ni wires with diameters ranging between 40 and 100 nm have shown that the reversal process occurs as the result of the nucleation of a single domain with a volume 200 times smaller than the volume of the entire wire.[12] So, it seems clear now, that, even for systems with weak crystal anisotropy, the reversal mechanism for real elongated particles (with finite length) cannot be described in terms of ''coherent'' modes such as ''curling'' and ''buckling'' [14] but seems to be well described in terms of nucleation-propagation reversal mechanisms. Nevertheless, despite the noncoherent character of the magnetization reversal mechanism found, the measured angular dependence of the switching field for Ni wires seems to be in good agreement with that found for the ''curling'' mode in infinite cylinders, although the fitted value for the exchange length λ_{ex} (about 17 nm) is smaller than that found in the literature (about 21 nm) [$\lambda_{ex}=(A/M_s^2)^{1/2}$, with A the exchange stiffness constant and M_s the saturation magnetization]. Thus, although the infinite cylinder model gives a first approximation to the nucleation mechanisms and the switching fields of an elongated particle, the deviations between the experimental values and those predicted for the infinite cylinder show that we should avoid the use of simple models to describe correctly the magnetization reversal mechanisms (and so, the

switching field values) occurring in elongated particles, even for ferromagnetic systems with low crystal anisotropy.

In contrast to Ni wires, Co nanowires display a more complex behavior because of the large crystal anisotropy resulting from the hexagonal close packed (hcp) growth of Co inside the pores. For this particular case, no analytical micromagnetic models exist, not even for simple geometries (infinite cylinder), and large scale micromagnetic calculations are needed to account for the observed properties.

The present work is mainly devoted to the study of the magnetization configurations and magnetization processes in Co and Ni nanowires. In the first part of this work, we report on magnetization, torque and magnetoresistance investigations of magnetization processes occurring in Co and Ni electrodeposited nanowires. These results are linked to the crystalline structure of the elaborated nanowires that has been investigated by transmission electron microscopy.[15] First conclusions drawn from the experimental work are corroborated in the second part of this article by large scale micromagnetic simulations for Co and Ni elongated bars with high aspect ratio. Moreover, these simulations have allowed us to explore in detail the magnetization reversal mechanisms in these systems and to compare them both to classical magnetization processes derived for the infinite cylinder and to previous experimental results on elongated particles.

II. FABRICATION OF ARRAYS OF MAGNETIC NANOWIRES

Random arrays of Co and Ni nanowires were fabricated by electrodeposition of Co (or Ni) in nanoporous track-etched membranes of polycarbonate following the same experimental procedure as the one described by Withney *et al.*[10] However, in the present work, we use ''homemade'' polycarbonate membranes exhibiting better properties in terms of pore orientation, pore surface roughness, pore shape, and pore size distribution.[16] In commercially available porous membranes, the angle between the pore axis and the normal to the film ranges typically between 0° and 30°. In our samples, the polymer film is bombarded perpendicular to the film and the angle is less than 10°. Also, the etching process following the irradiation was optimized to produce a uniform cross section all along the pore length with very small roughness since in commercially available porous membranes the pore shape often exhibits deviations from the ideal cylindrical shape, such as toothpick shape or constriction at the middle of the channels. The reduced roughness of the pore walls is also particularly crucial for the membranes with the smallest diameter. Furthermore, we report here only results for arrays of Ni and Co wires prepared using membranes of low porosity, where the average spacing between the wires is much larger than 1 μm and interactions between magnetic elements are expected to be small.[17] Deposition into the pores of the membrane is monitored through the measurement of current and stopped as soon as the pores have been filled completely. In these conditions the average final length of the wires (10 or 20 μm) equals the thickness of the membranes and their diameter ranges between 35 and 500 nm.

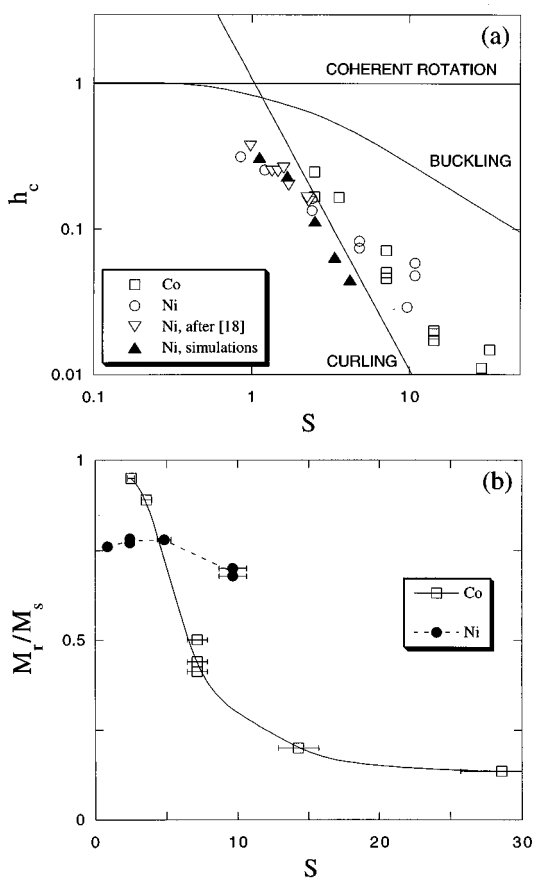

FIG. 1. (a) Room-temperature reduced coercive field $h_c = H_c/2\pi M_s$ as a function of the reduced radius for Ni (O) and Co (□) (the error bars are included in the size of the symbol). Values obtained for a single Ni wire by Wernsdorfer *et al.* (Refs. 12 and 18) are shown separately (▽) (the error bars are included in the size of the symbol). These results are plotted together with the results of micromagnetic simulations for zero anisotropy systems (▲). All these values correspond to the hysteresis loops recorded with the field applied parallel to the wires. Solid lines denote the theoretical values of the nucleation field for the three possible nucleation modes in the infinite cylinder (after Ref. 14). (b) Room-temperature normalized remanent magnetization (squareness) for Ni and Co wires as a function of reduced radius obtained for an applied field parallel to the wires.

III. EXPERIMENTAL RESULTS: STATIC MAGNETIZATION, TORQUE, AND ANISOTROPIC MAGNETORESISTANCE

Magnetization and torque measurements were made on the whole system membrane wires in order to take advantage of both the orientation of the wires inside the membrane and of the protection against oxidization provided by the polycarbonate membrane. This configuration also allows the use of standard magnetometry techniques.

Figure 1(a) shows the variation of the reduced coercive field $h_c = H_c/2\pi M_s$ for both Co and Ni nanowires as a function of the reduced radius $S = R/(A/M_s^2)^{1/2}$ for a magnetic field applied parallel to the wires. The ''reduced'' plot allows us to compare correctly in a single figure two or more systems with different magnetic characteristics (as is the case for Ni and Co) and to obtain a general picture for the

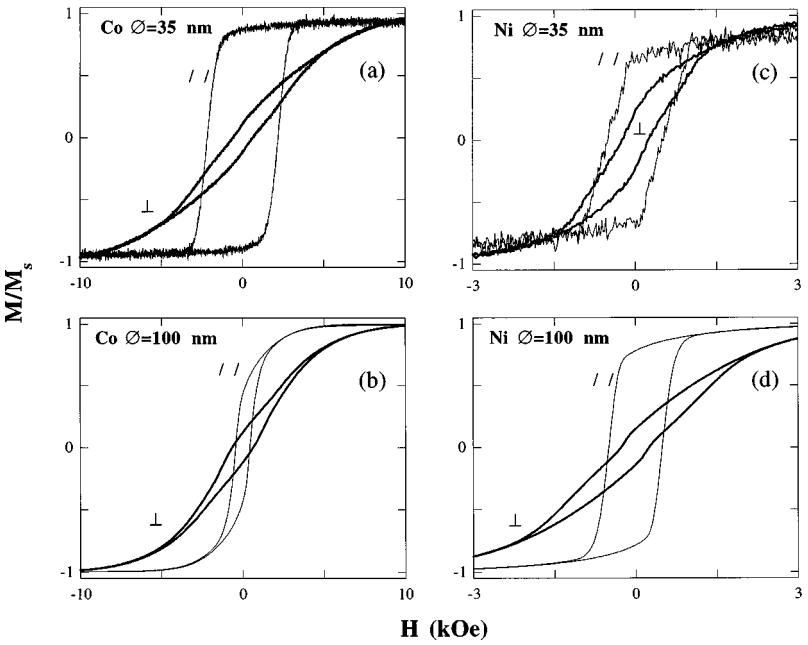

FIG. 2. Hysteresis loops at room temperature for Co (a,b) and Ni (c,d) wires recorded with the field applied parallel (∥) and perpendicular (⊥) to the wire. Results are given for the 35 nm (a) and 100 nm (b) Co wires and for 35 nm (c) and 100 nm (d) Ni wires.

size dependence of elongated particle switching fields. We also report reduced switching field values recorded by Wernsdorfer *et al.* on a single Ni wire using a microSQUID.[18] The reduced radius has been calculated assuming bulk Ni and Co saturation magnetizations [M_s(Ni)=480 emu/cm^3 and M_s(Co)=1400 emu/cm^3] and the exchange length λ_{ex} to be of 7 nm for Co and 21 nm for Nickel.[19] With the experimental results, we plot the predicted curve for curling, buckling, and coherent rotation reversal modes calculated for infinite cylinders[14] and the results of our micromagnetic calculations for wires with zero crystal anisotropy (good approximation for Ni). The measured coercive fields in both Co and Ni wires exhibit a large increase as the radius decreases. Although h_c takes on values that are not far from those predicted by the curling or buckling nucleation mechanism in the infinite cylinder, the tendency of h_c does not agree with any one of the nucleation mechanisms proposed. Comparing the values of h_c obtained from micromagnetic simulations to the measured data, we find a good agreement for Ni wires with small diameters. For large wire diameters the calculated coercivities deviate from the measured values, the simulated h_c being slightly smaller than the measured h_c. Comparing measurements of the coercive fields carried out in Co wires with those measured for Ni wires we observe a different behavior for large and small diameters. For large diameters ($S>5 \Leftrightarrow \varnothing_{Co}>50$ nm), h_c in Co wires takes on values comparable to those measured on Ni wires. For small diameters, the measured reduced coercive fields in Co wires are higher than those measured for Ni wires.

Figure 1(b) shows the variation of the remanent magnetization as a function of the reduced radius. For Co nanowires, the squareness (M_r/M_s) decreases from a value close to 1 for the smallest diameter (35 nm) to 0.1 for a diameter of 500 nm, while for Ni the remanent magnetization remains close to 0.8 for the whole diameter range. Again, large and small diameter Co wires compare differently to Ni wires. In Ref. 10, a decrease of the squareness with increasing diameter was observed for arrays of Ni wires with pore density of about 6×10^8 cm^{-2}. In a previous work, we also found such a decrease when the array of Ni wires was formed using membranes samples of similar porosity.[17] We thus conclude that this effect results from dipole-dipole interactions and that the data shown in Figs. 1(a) and 1(b) are closer to that of isolated magnetic nanowires over the whole diameter range.

Qualitatively, the origin of these observed features can be understood in the light of a simple model: the infinite cylinder. For infinite cylinders, the shape anisotropy tends to force the magnetization to be along the rod axis. In the case of zero crystal anisotropy, micromagnetic theory predicts only three types of nucleation (and reversal) mechanisms: coherent rotation, buckling, and curling.[14] All these reversal modes should result in a square hysteresis loop when the field is applied parallel to the cylinder axis. For a parallel-to-cylinder easy axis of crystal anisotropy, this term reinforces the shape contribution and again only square hysteresis loops can occur, the switching field being higher than for zero crystal anisotropy.[14] Square hysteresis loops have been observed for the whole diameter range explored in Ni nanowires but only for small diameters (35 and 50 nm) in Co wires [Figs. 2(a)–2(d)]. The decrease of remanence for large diameters in the Co systems can be understood in the light of x-ray diffraction and transmission electron microscopy experiments.[15] Diffraction patterns of Co nanowires indicate that Co is stabilized in the hcp structure with a preferential (0001) texture oriented close to the direction perpendicular to the axis of the wires. Moreover, an analysis of the microstructure in Co wires reveals the presence of very well (0001) oriented single crystals several μm long. As a result, there is a large crystal contribution to the anisotropy energy (for bulk hcp cobalt $K_1\approx4.5\times10^6$ erg/cm^3) that favors an orientation of the magnetization along the c axis, perpendicular to the wire. This term competes directly with the shape anisotropy ($\approx\pi M_s^2=6\times10^6$ erg/cm^3) that favors an orientation along the axis of the wire. This peculiar orientation of the crystal easy axis in Co wires explains the strong decrease of the remanent magnetization when the wire diam-

eter increases. Moreover, the observed quasi-perpendicular-to-wire orientation of the Co hcp *c* axis and the shape of the hysteresis loops for large diameters [Fig. 2(d)] suggest that, for small applied fields, the magnetization of the wire tends to split into domains partially oriented perpendicular to the wire axis.

A possible explanation of the large values of the coercive field and the remanent magnetization for Co wires with small diameter comes from recently undertaken microstructural analysis.[20] Apparently, extended x-ray-absorption fine structure (EXAFS) experiments show a change in texture with the pore size. Thus, for large pore sizes, the Co hcp *c* axis would lie perpendicular to the wire while for extremely small pore diameters its orientation would be along the wire axis.

To quantify the variation of the crystal anisotropy, torque experiments for Co wires have been carried out for diameters ranging between 50 and 400 nm. We have recorded the torque due to the applied magnetic field both for the field rotating in the plane of the membrane (in-plane) and in the plane perpendicular to the membrane (out-of-plane). The applied field was 10 kG, large enough to ensure a quasisaturated state with the magnetization within 5° of the field for all angles. Measurements with an in-plane rotating field do not show any remarkable features, indicating that, on the average, the system membrane wires is isotropic in the plane of the membrane. This agrees with the intuitive idea that even if every Co single crystal has its own orientation for the hcp *c* axis, the distribution of *c* axis in the membrane should not present, *a priori*, any preferred orientation. Measurements in the out-of-plane configuration show more interesting features since both shape and crystal anisotropy contribute to the signal.

For all diameters studied, the torque measurements indicated that the overall easy direction for uniform magnetization lies along the wire axis. For diameters larger or equal to 100 nm the hard direction has been found to be the direction perpendicular to the wire. Fitting the torque data with a Stoner Wohlfarth model[21] (good approximation for high fields[22]) has enabled us to determine the dependence of the anisotropy constants on the wire diameter. Approximate values obtained for K_1 for Co at room temperature are shown in Fig. 3. The large error bars in these values come from the uncertainty in the total volume of the ensemble of magnetic wires. For 50 nm large Co wires, the first-order crystal anisotropy constant is about 2×10^6 erg/cm^3, which is smaller than the bulk value, showing a rapid increase in magnitude from 100 to 200 nm and stabilizing for a value slightly higher than the bulk value (about 6×10^6 erg/cm^3) for large wire diameters. So, K_1 compares only to the demagnetizing energy, near πM_s^2, for very large samples.

For the smallest wire diameter measured (50 nm), an extremely small value of K_1 has been found. This fact coincides with the change in behavior observed for the coercive field and the remanent magnetization for small diameters in Co. The change in orientation of the Co hcp *c* axis from perpendicular to wire for large diameters to parallel to wire for small diameters concluded from EXAFS experiments[20] would also agree with the measured torque data. We can estimate the mean angle separating the crystal anisotropy axis from the direction perpendicular to the wire (ψ) for 50 nm Co wires with a simple model. Assuming the absolute

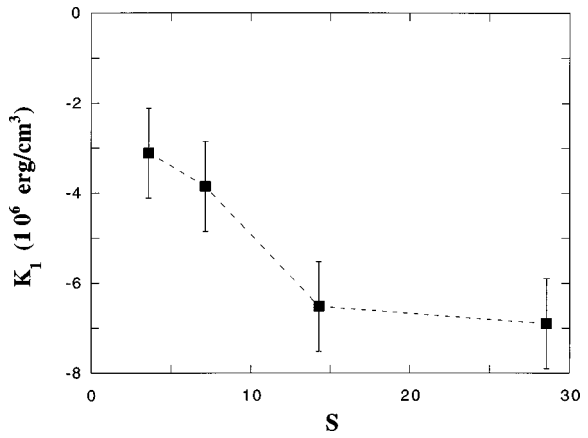

FIG. 3. Fitted values of the first-order crystal anisotropy K_1 as function of the reduced radius. These values have been obtained fitting torque measurements for Co wires with the Stoner-Wohlfarth model.

value of K_1 to be equal to that measured for large diameters, the measured torque value should correspond to a value of the effective first-order anisotropy of $K_1(\frac{1}{2}\cos^2\psi-\sin^2\psi)$. Applying this formula we obtain a value for ψ of the order of 20–25°, and we find that the critical value of ψ for a zero crystal anisotropy contribution to the torque is close to 35°. Thus, if the change in orientation of the hcp *c* axis continues as the diameter decreases, for very small diameters we can expect a large contribution of the crystal anisotropy along the wire axis. This contribution could explain the coercive fields and remanence measured for small diameter Co wires, whose values are higher than those measured for Ni wires for which only a demagnetizing contribution to the overall anisotropy exists.

While magnetization and torque measurements give some indirect insights into the magnetization reversal mechanisms in Co nanowires, resistivity measurements as a function of the applied field provide microscopic information on the alignment of the magnetic moments on the length scale of the electronic mean free path. In Fig. 4 we show typical magnetoresistance measurements obtained for the system membrane wires, with the electric current flowing along the wires and the magnetic field applied both along the wires and perpendicular to the wires. Figure 4(a) corresponds to measurements on an array of Co wires with diameters about 90 nm. The magnetoresistance (ρ/ρ_0) exhibits a negative variation when the field is applied parallel to the current, while the effect is reversed when the field is perpendicular to the current. This can be understood in the framework of the anisotropic magnetoresistance (AMR) phenomenon related to the change in the orientation between magnetization and current.[23] Similar results have been obtained for arrays of Co wires with larger diameters (200 and 450 nm). These observations corroborate the presence at zero field of a multidomain configuration with the magnetization of each domain partially oriented along the normal to the wire. This result agrees with the intuitive argument suggested above to explain magnetization measurements for large Co wires.

In contrast, for thin Co wires (35–50 nm), no change in resistivity has been observed with the magnetic field applied parallel to the wire axis [Fig. 4(b)]. This behavior coincides

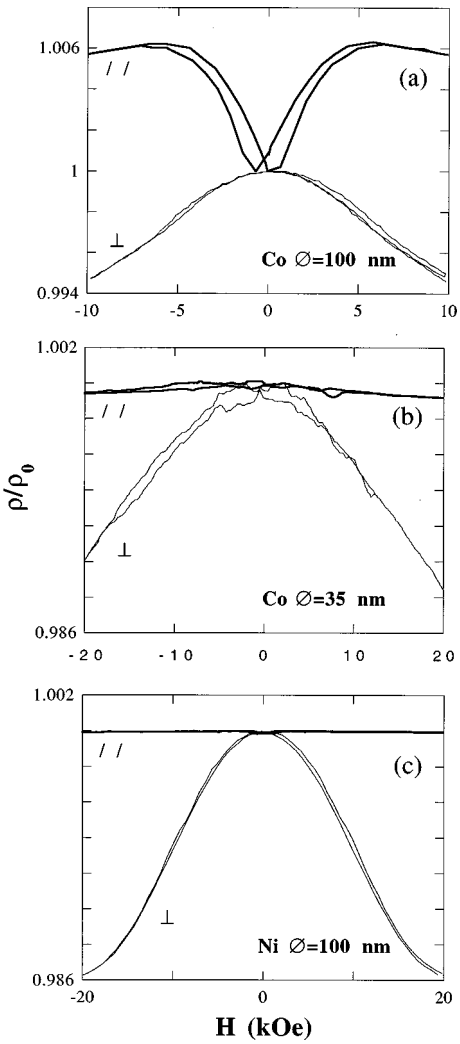

FIG. 4. Resistivity vs field measurements at room temperature for Co (a,b) and Ni (c) wires recorded with the field applied parallel (∥) and perpendicular (⊥) to the wire. Curves shown correspond to 35 nm (a) and 100 nm (b) Co wires, and to 100 nm Ni wires (c).

with that observed over the whole diameter range for an array of Ni wires [Fig. 4(c)].[17] Since the resistivity would vary with the applied field if the magnetization of each wire split into domains, a constant resistivity suggests that the only stable magnetization configurations of each wire are single domain (or, at least, that the deviations from a single domain configuration are negligible). The observed small differences between the measured hysteresis loops and a square loop certainly have their origin in both a small dispersion in wire diameter and a weak magnetostatic contribution appearing from the dipole-dipole interactions between wires.

IV. RESULTS OF MICROMAGNETIC CALCULATIONS

To complete our understanding of the magnetization processes in very thin wires, large scale micromagnetic calculations have been carried out for thin wire diameters. The micromagnetic simulation method employed here has been described extensively elsewhere.[24]

A rapid overview of previous reported theoretical results permits us to realize that there should be significant differences between the finite and the infinite cylinders. For an infinite cylinder with dominant shape anisotropy, it has been shown theoretically that the most probable magnetization reversal mechanisms are curling and buckling (uniform rotation can be regarded as the limit of buckling as cylinder diameter goes to zero).[14] For a finite cylinder with small anisotropy, as it holds for a prolate spheroid,[25] we would expect rotation in unison to exist for very small but finite diameters while buckling and curling should be observed for intermediate and large diameters, respectively. Since the results obtained for infinite (and finite) cylinders do not differ much from those obtained for infinite (finite) bars,[26] we have taken, as a matter of numerical effectiveness,[24] the latter geometry to represent the wires. The shape of the extremities has been taken arbitrarily to be flat since their role is only important for low aspect ratio (around 5) bars and for applied fields with less than 1° of misalignment to the bar axis.[27] The simulated wires have an aspect ratio of 25, and the applied field has been taken to form an angle of 1° with the wire axis since, as it has been mentioned above, the wires in the membrane are not perfectly aligned. So, the effects of the particular shape of the extremities of the wires are negligible.

To study the reversal mechanisms in finite cylinders (or prisms) and confront them with those derived analytically for infinite cylinders and prolate spheroids (for zero anisotropy), Ni wires are the most appropriate systems because of their small crystal anisotropy. We have simulated the reversal process in Ni wires by means of micromagnetic calculations for bars with square cross-section, with reduced widths $a/[2(A/M_s^2)]^{1/2}$ ranging between 1 and 4.5 and an aspect ratio (length to width ratio) of 25. The reduced dimension of the elementary cell in the simulations ranges between 0.2 and 0.5, small enough compared to 2 (the critical characteristic length for nonuniform magnetisation is close to $2\lambda_{ex}$) in order to ensure a good description of the magnetization in the system.[28] Crystal anisotropy has been assumed to be zero.

For very thin bars, only square hysteresis loops have been obtained from simulations. Moreover, a noncoherent reversal mechanism similar to buckling and starting at one end of the wire has been found to have the smallest nucleation field and so to be the most probable reversal mechanism. The values of the switching field for this reversal mechanism compare favorably with those observed for small diameter Ni wires [Fig. 1(a)]. Dynamical micromagnetic simulations[29] have allowed to calculate the evolution with time of the magnetization configuration. The transient configurations during the reversal process are shown in Figs. 5(a)–5(d). The first phase (and the slowest one) of the magnetization reversal process consists in the nucleation of a reversed domain at one extremity of the wire [Figs. 5(a) and 5(b)]. This first nucleation process is accompanied by a new domain nucleation in the neighboring region, activated by the change in stray field produced by the first domain nucleation [Fig. 5(c)]. The domain nucleation ''avalanche'' continues until the whole magnetization of the wire has been reversed. The main result obtained from these simulations is that the nucleation process and the magnetization reversal are initiated by the nucleation of one reversed domain at one extremity, its size being less than three times the exchange length of the material, that is involving a volume of less than $12\lambda_{ex}^3$ [for Ni

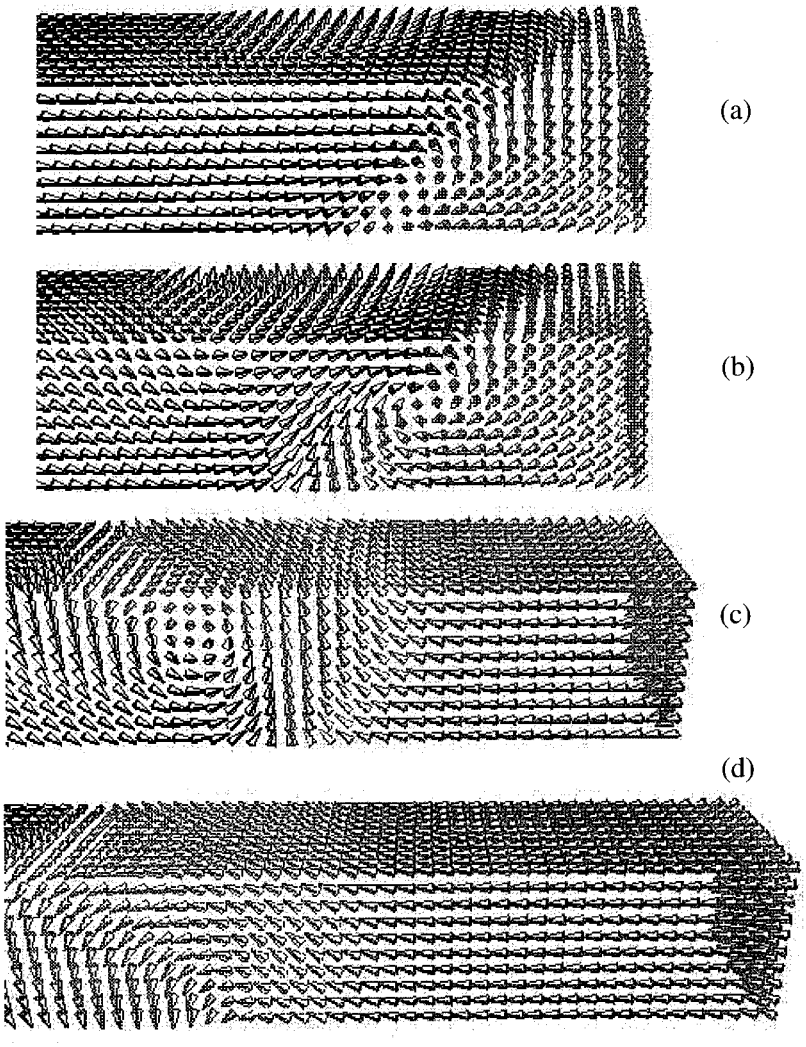

FIG. 5. Magnetization reversal in zero anisotropy wires for a reduced width $S=1.5$. Figures (a)–(d) correspond to successive images of the magnetization of the wire in ''chronological'' order for a reduced applied field of 0.23 (nucleation field). Reversal starts with the creation of a reversed domain at one extremity of the wire (a) followed by the nucleation of other domains deeper inside the wire (b,c,d). Although the whole process is triggered by a single domain nucleation at one end, this reversal mechanism does not correspond to a wall displacement but to a bucklinglike process since the walls that created at a point in the wire do not displace. They rather cross the wire and disappear.

$12\lambda_{ex}^3=(45\ \mathrm{nm})^3$]. An exact measurement of the volume of the initially reversed domain through the calculated value for the magnetisation gives a domain size of about $(32\ \mathrm{nm})^3$. The most important result extracted from this nucleation mechanism derives from the analysis of the stability of the initially nucleated domain. We have taken the nonequilibrium magnetization configuration in Fig. 5(a), obtained for an applied field equal to h_c, and we have changed ''instantaneously'' the field to a value smaller than h_c but pointing in the same direction. After that, the simulation procedure was restarted and the stability of the artificially created new magnetization state was tested. In all the cases explored, we have found that this configuration was unstable and that the reversal progressed until the total magnetization of the wire was reversed. So, comparing this computer ''experiment'' to thermally activated reversal, we can ensure that the nucleation of a domain of size around $(32\ \mathrm{nm})^3$ at one extremity is always accompanied by the complete reversal of the magnetization of the wire. Thus, the calculated domain volume should be larger than (or at least equal to) the activation volume and so it gives an upper bound for the activation volume in Ni wires. As expected, the value found is larger (but of the same magnitude order) than the $(20\ \mathrm{nm})^3$ determined by Wernsdorfer *et al.*[12] from thermally activated magnetization reversal measurements in Ni wires.

For Ni wires with large diameter the simulations reveal a different, most probable, magnetization reversal mechanism. For this size range we can distinguish two critical fields. The first is the nucleation field (h_n), at which the magnetization of the system deviates from saturation. The second is the switching field (h_s), at which an irreversible magnetization jump occurs. Dynamic simulations of the magnetization reversal have shown that departure from saturation takes place at both extremities of the wire according to the curling mode [Fig. 6(a)][14] while far from the extremities the magnetization remains oriented along the wire axis. After curling nucleation at both extremities, reducing the applied field results in a propagation of the nucleated vortices inwards until $h=h_s$, where the magnetization of the wire reverses completely according to a domain nucleation and domain-wall propagation mechanism [Fig. 6(b)]. As it could be expected, the calculated values of the switching field (coercive field) for this size range are very close to those of the curling mode in infinite cylinders. However, it is for this size range that the agreement between calculated and measured values of the coercive field is worst. It is important to notice that it is also for this size range that the coercive field takes on the smallest values. Thus, other effects not taken into account in the calculations such as pinning at defects and/or interactions between wires inside the membrane could become important

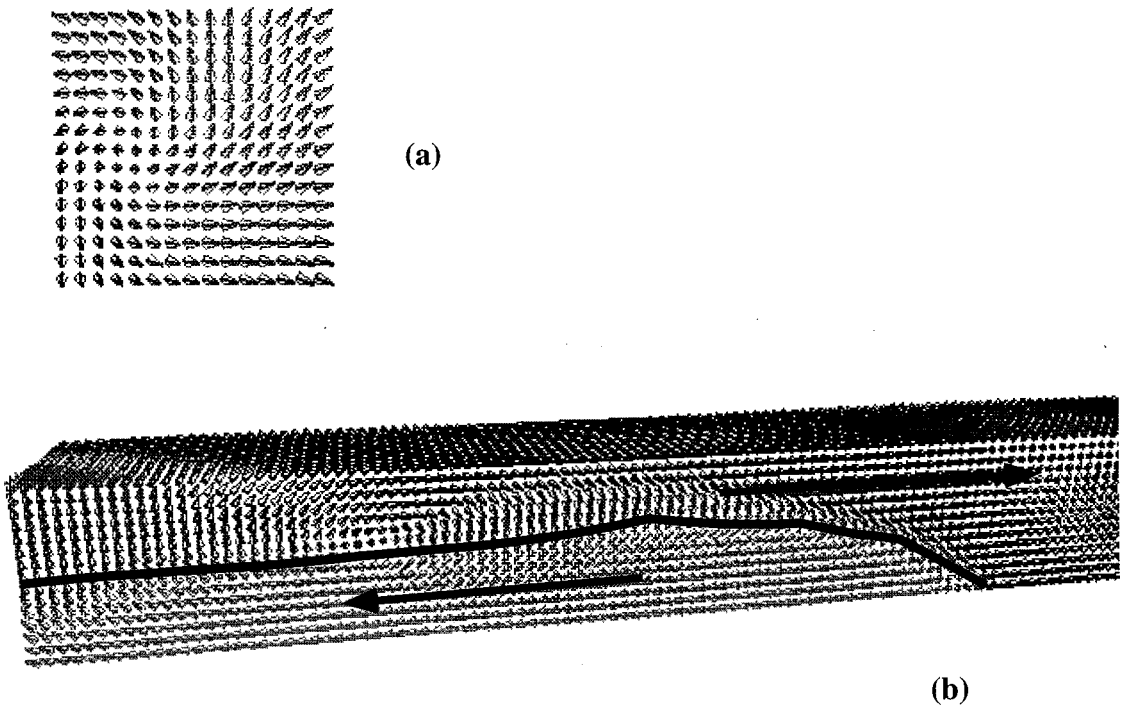

FIG. 6. Nucleation and magnetization reversal mechanism for a $S=2.35$ Ni wire. In Fig. (a) is shown the magnetization configuration at one of the extremities after nucleation. As shown first deviations from uniform magnetization take place with the creation of one magnetization vortex at each extremity of the wire. Figure (b) shows a transient state during the magnetization reversal for an applied field equal to the switching field. According to this figure the magnetization reversal occurs as a consequence of the nucleation of a reversed domain at one side of the wire and the displacement of the created domain wall across the wire.

for this size range. Pinning fields or stray fields, comparable in value to the switching fields, could alter appreciably the reversal mechanism and, consequently, the measured value of the coercive field.

In order to figure out the way the magnetization reversal takes place in Co wires and to clarify the influence of the observed orientation of the hcp *c* axis we have also undertaken large scale three-dimensional (3D) micromagnetic simulations of these systems. We assume the wires to be single crystal with the *c* axis oriented perpendicularly to the axis of the wire. As a matter of simplicity, we have only simulated wires with a square cross section instead of the observed circular one, since this does not significantly alter the calculated properties.[26] The parameters of the simulation are those of bulk hcp cobalt, i.e., an exchange length λ_{ex} of 70 Å, and a saturation magnetization (M_s) of 1400 emu/cm^3. The reliability of these simulations is determined by the size of the elementary domains (of cubic shape) in comparison to the characteristic sizes defining the micromagnetic problem, i.e., domain size and domain-wall thickness. We have fixed the width of the elementary cubic domains to 3 nm, quantity to be compared to twice the exchange length (14 nm) and to domain-wall thickness (of the order of $\pi\sqrt{A/K}\approx 16$ nm for $K_1=5\times10^6$ erg/cm^3).

For cobalt wires, the strong shape anisotropy competes with the crystalline anisotropy. What we expect from the combination of these two anisotropy contributions is a modification of the magnetization reversal mechanism and consequently a change in the evolution of the switching field vs size in comparison to what has been found for small crystal anisotropy (Ni wires). As it has been discussed above, the particular microstructure of thin Co wires gives rise to a change in the crystal anisotropy and particularly to a reduction of the effective perpendicular-to-wire anisotropy compared to that measured for large diameters. To see how the reversal mechanism and consequently the magnetization curve is affected by the reduction of the perpendicular-to-wire anisotropy, we have first studied two magnetic configurations corresponding to two different values of the first-order crystal anisotropy (5×10^6 erg/cm^3 and 10^6 erg/cm^3), close to the values obtained experimentally, and always oriented along the normal to the wire. The hysteresis loops for two simulated single-crystal Co wires 30 nm wide and with $K_1=5\times10^6$ erg/cm^3 and $K_1=10^6$ erg/cm^3, respectively, and calculated with an applied field along the wire axis are shown in Fig. 7. For $K_1=5\times10^6$ erg/cm^3 the strong crystal anisotropy favors the nucleation of a nonuniform magnetization configuration at a positive field of about 2 kOe. The nonuniform rotation of the magnetization in the upper branch of the hysteresis loop occurs through a bucklinglike process giving rise to the appearance of domains with alternate orientation at remanence [Figs. 8(a)–8(c)]. The most interesting feature is the strong influence of the extremities of the wire on the orientation and the size of the domains. Close to the ends, the domains tend to orient fully along the crystal anisotropy axis. This effect and the absence of a domain wall at the extremity of the wire, gives rise to an appreciable widening of the domains (the width of the domain at the extremity is around 80 nm) and to the appearance of mixed Néel-Bloch walls (or vortex walls)[29] in between with a characteristic size of 15 nm, measured at the center of the domain wall [Fig. 8(b)]. However, at the center of the wire,

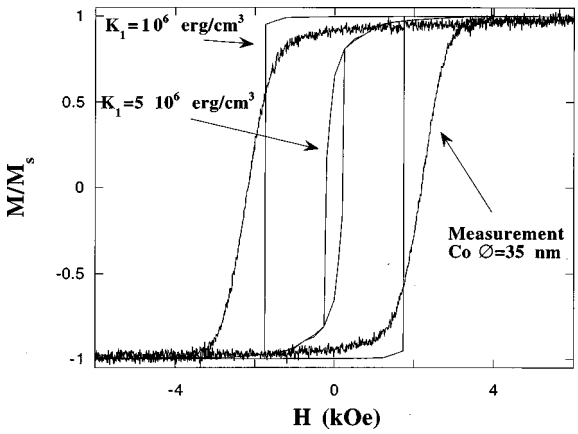

FIG. 7. Simulated hysteresis loops for Co wires with the field parallel to the wire obtained for a fixed wire width of 30 nm and two different values of the second-order anisotropy constant 5×10^6 erg/cm^3 and 10^6 erg/cm^3. These curves are plotted together with the measured hysteresis loop for a 35 nm Co wire.

the magnetization inside the domains tends to align nearly completely along the wire axis with only small components parallel to the anisotropy axis. In this case, the observed domains are smaller (around 30 nm including the domain wall) and the walls separating them are of the Néel type [Fig. 8(c)]. For a smaller value of the crystal anisotropy $K_1=10^6$ erg/cm^3, the magnetization of the wires remains mostly parallel to the wire axis until the reverse applied field is increased above 1800 Oe at which an irreversible jump takes place (this value of the switching field is only 100 Oe smaller than that calculated for a zero anisotropy Co wire). Dynamic simulations of this reversal process have shown a reversal mode of buckling type similar to that shown in Fig. 5 for zero crystal anisotropy. A close look to the calculated hysteresis loops shows that (i) the coercive field is much larger for $K_1=10^6$ erg/cm^3 than for $K_1=5\times10^6$ erg/cm^3 (approximately by a factor of 10); (ii) the remanence is close to one for $K_1=10^6$ erg/cm^3 while it drops rapidly when increasing the anisotropy constant to reach a value of 0.65 for $K_1=5\times10^6$ erg/cm^3; (iii) for $K_1=5\times10^6$ erg/cm^3 the magnetization tends to split into domains at low fields, while for $K_1=10^6$ erg/cm^3 the magnetization lies oriented along the wire for the whole field range. Comparing the results obtained from simulations to measured hysteresis loops and resistivity curves for thin Co wires, it seems clear that only a reduction of the effective perpendicular anisotropy can explain the experimental results obtained for 35 and 50 nm Co wires.

The question whether this reduction of the effective perpendicular anisotropy could be the result of a reorientation of the c axis from perpendicular-to-wire for large Co wires to parallel-to-wire for thin Co wires has also been checked by means of micromagnetic simulations. These simulations have been undertaken only for wires of small widths (35

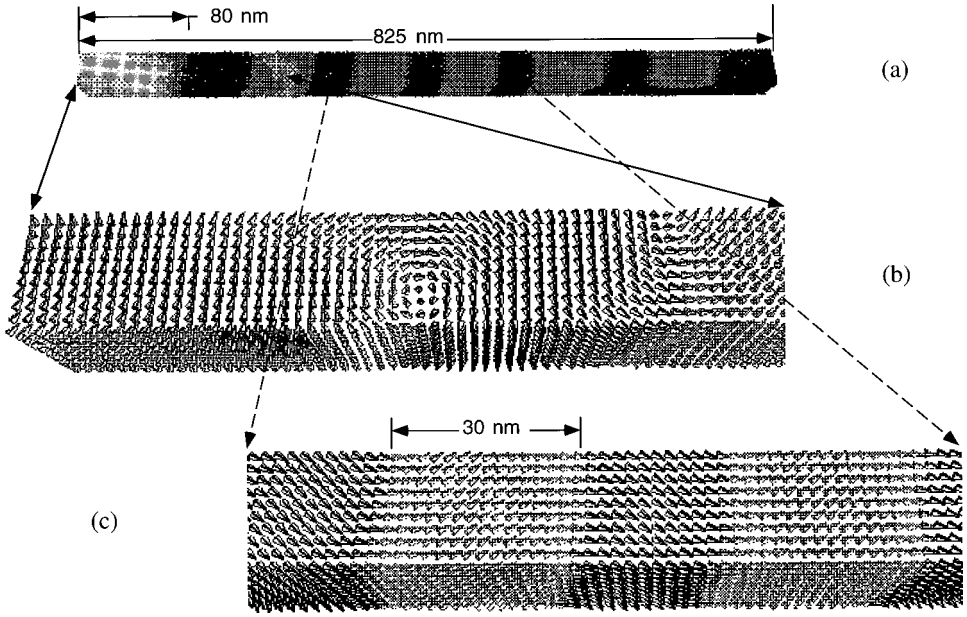

FIG. 8. (a) Equilibrium magnetization configuration at zero field (remanent magnetization configuration) for a simulated Co wire 30 nm in diameter. The crystal anisotropy constant is here 5×10^6 erg/cm^3. Figures (b) and (c) show details of the magnetization configuration at the end and the center of the wire respectively. Gray contrast indicates an up (light gray) and a down (dark gray) oriented magnetization. Notice the difference in orientation (contrast) and size between the domains at the end of the wire and the domains at the center. While at the ends the magnetization tends to orient along the crystal anisotropy axis (perpendicular to wire) at the center the magnetization is mostly oriented along the wire and only a small oscillatory component along the crystal anisotropy axis appears.

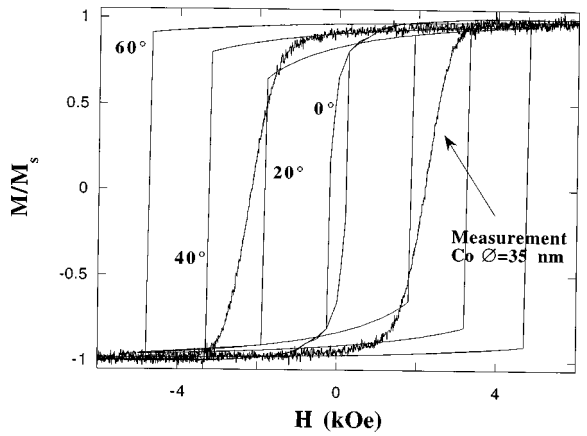

FIG. 9. Simulated hysteresis loops for a 35 nm Co wire with a first-order crystal anisotropy constant 5×10^6 erg/cm^3 and for different values of the angle formed by the *c* axis (crystal anisotropy easy axis) and the normal to the wire axis ranging between 0° and 60°. To facilitate the comparison with the experimental results, we plot together the hysteresis loop recorded for an ensemble of Co wires with 35 nm diameter.

nm). We have assumed the value of the anisotropy constant to be $K_1=5\times10^6$ erg/cm^3 and the angle between the anisotropy axis and the normal to the wire to range between 0° and 60°. The simulated hysteresis loops obtained are shown in Fig. 9, together with the experimental hysteresis loop for 35 nm Co wires. These results show strong differences in switching field among the simulated hysteresis loops for small angles between the *c* axis and the normal to the wire (0°–60°). For large angles, the hysteresis loops tend vs a rectangular loop and the coercive fields increase to take values much larger than the measured ones. For very small angles (0°–20°), the simulated hysteresis loops present lower remanent magnetization and coercivities than the measured ones. This permits to affirm that for small wire diameters, the growth conditions favor an orientation of the hcp *c* axis that differs from that observed for larger Co wires.[15] Moreover, since the coercive fields for the simulated hysteresis loops with highest deviations of the *c* axis are larger than the measured one we can conclude that, for very small Co wire diameters (35 nm), a strong reorientation of the anisotropy axis towards the wire axis (at least of about 30°) should take place.

To date, the problem of the crystallographic orientation of plated Co films is still controversy. Previous studies have shown that the orientation of the *c* axis can be drastically affected by electrodeposition conditions such as the *pH* of the electrolyte solution and plating current density[30] and even by electrolyte temperature.[31] We may also argue for non conventional growth in very confined media. At this stage, it is not possible to discriminate between the numerous possible mechanisms responsible for such a reorientation effect. We address this important point to future work.

V. CONCLUSIONS

In summary, we have studied the reversal mechanisms in cobalt and nickel nanowires. Since nickel wires present a very small crystal anisotropy their study has allowed us to check the predictions arising from infinite cylinders. From magnetization and resistivity measurements it has been proved that the magnetization reversal in Ni wires with small diameter takes place in a single magnetization jump. A detailed micromagnetic study of this system has allowed to describe correctly the reversal mechanisms for small diameter Ni wires. For this size range a good agreement has been found between the calculated and the measured coercive fields for an array of wires inside a polycarbonate membrane as well as for single wire measurements on microSQUIDS.[12,18] For increasing Ni wire diameter, both the calculated and the measured switching fields decrease. However, for large diameter the coercive fields measured on the ''wire ensemble'' deviate both from those predicted by micromagnetic simulations and from the curling nucleation fields in the infinite cylinder. One possible explanation for this behavior is the following: Since the ''intrinsic'' switching field decreases with diameter, for large diameter it becomes very small and comparable to the magnetostatic (stray) field. In this case, the deviation (notice that this deviation is only of a few tens Oe) could be due to a combined effect of the interactions between wires in the membrane and the intrinsic switching fields. An alternative explanation is to consider that the grain boundaries act as pinning centers and give rise to small pinning fields, whose influence should be only noticed for large diameters. Since single-wire measurements on large diameter Ni wires reported by O'Barr and co-workers[13] show the same disagreement between measured switching fields and analytical values for the curling nucleation fields, the second hypothesis drawn above to explain the origin of the deviations seems to be the most acceptable one. Thus, for large diameter the magnetization reversal would consist in a stepwise wall displacement between grain boundaries instead of the single-step wall displacement found by micromagnetic simulations.

In contrast, cobalt nanowires present a strong crystal anisotropy with an easy axis oriented nearly perpendicular to the axis of the wire, at least for large diameters. For small diameters, Co wires behave all along the hysteresis loop like a single domain with an easy axis along the wires. Resistivity measurements show that magnetization reversal takes place as an irreversible jump in each one of the wires independently and micromagnetic calculations show that this process takes place starting with a domain nucleation. This behavior is similar to that found for Ni wires in the whole range of diameters studied. Comparing the simulated hysteresis loops with the experimental data, it seems clear that small diameter Co wires present a reduction of the effective perpendicular to wire crystal anisotropy in comparison to the bulk value. Also, according to measured coercive fields, torque experiments, and micromagnetic simulations for Co wires with different orientations of the hcp *c* axis, a change in orientation of the *c* axis of about 30° away from the wire normal is the most convincing explanation for this observed reduction of the effective perpendicular anisotropy. Finally, for large Co wire diameters, magnetization and resistivity measurements prove the existence of a multidomain magnetization configuration, each domain being oriented partially along the perpendicular to the axis of the wire. This orientation of the magnetization results from the increasing value of the effective perpendicular anisotropy with wire diameter.

ACKNOWLEDGMENTS

We thank Whatman S.A. (Belgium) and the Unité des Hauts Polymères at UCL for providing the polycarbonate membranes used in this study. We would also like to thank W. Wernsdorfer for sending unpublished measurements of switching fields in Ni nanowires and P. Lefebvre for sending us information on microstructural analysis in Co nanowires prior to publication. Special thanks are given to the CNCPST and the IDRIS for the use of their computing facilities. This work was supported by a Brite-EuRam program of the European Commission (BE95-1761) and the Belgian Interuniversity Attraction Pole Program (PAI-IUAP P4/10).

*Corresponding author. FAX: (33) 3 88 10 72 49; Electronic address: ricardo@taranis.u-strasbg.fr

[1] W. F. Brown, *Magnetostatic Principles in Ferromagnetism* (North-Holland, Amsterdam, 1962); *Micromagnetics* (Wiley-Interscience, New York, 1963).

[2] C. R. Morelock, Acta Metall. **10**, 161 (1962); S. S. Brenner, *ibid.* **4**, 62 (1956); F. E. Luborsky, T. O. Paine, and L. I. Mendelsohn, Powder Met. Bull. **4**, 57 (1959).

[3] F. E. Luborsky, J. Appl. Phys. **32**, 171S (1961).

[4] F. E. Luborsky and C. R. Morelock, J. Appl. Phys. **35**, 2055 (1964).

[5] A. Aharoni, in *Coherent and Incoherent Magnetisation Processes in Non-interacting Particles*, Vol. 338 of *NATO Advanced Study Institute, Series E: Applied Sciences*, edited by G. C. Hadjipaucyis (Kluwer Academic, Dordrecht, 1997).

[6] M. Hehn, K. Ounadjela, J. P. Bucher, F. Rousseaux, D. Decanini, B. Bartenlian, and C. Chappert, Science **272**, 1782 (1996); R. F. W. Pease and R. L. White, J. Vac. Sci. Technol. B **13**, 1089 (1995); G. A. Gibson and S. Schultz, J. Appl. Phys. **73**, 4516 (1993); S. Chou, P. Krauss, and L. Kong, *ibid.* **79**, 6101 (1996); M. Ledermann, S. Schultz, and M. Ozaki, Phys. Rev. Lett. **73**, 1986 (1994); T. Hirayama, Q. Ru, T. Tanji, and A. Tonomura, Appl. Phys. Lett. **63**, 418 (1993); E. Gu, E. Ahmad, S. J. Gray, C. Daboo, J. A. C. Bland, L. M. Brown, M. Rührig, A. J. McGibbon, and J. N. Chapman, Phys. Rev. Lett. **78**, 1158 (1997).

[7] C. R. Martin, Adv. Mater. **3**, 457 (1991), and references therein.

[8] S. Kawai and R. Ueda, J. Electrochem. Soc. **122**, 32 (1975).

[9] K. I. Arai, K. Ishiyama, Y. Ohoka, and H. W. Kang, J. Magn. Soc. Jpn. **13**, 789 (1989).

[10] T. M. Whitney, J. S. Jiang, P. Searson, and C. Chien, Science **261**, 1316 (1993).

[11] L. Piraux, J. M. George, J. F. Despres, C. Leroy, E. Ferain, R. Legras, K. Ounadjela, and A. Fert, Appl. Phys. Lett. **65**, 2484 (1994); L. Piraux, S. Dubois, and A. Fert, J. Magn. Magn. Mater. **159**, L287 (1996); S. Dubois, C. Marchal, J. M. Beuken, L. Piraux, J. L. Duvail, A. Fert, J. M. George, and J. L. Maurice, Appl. Phys. Lett. **70**, 396 (1997).

[12] W. Wernsdorfer, B. Doudin, D. Mailly, K. Hasselbach, A. Benoit, J. Meier, J.-Ph. Ansermet, and B. Barbara, Phys. Rev. Lett. **77**, 1873 (1996).

[13] M. Lederman, R. O'Barr, and S. Schultz, IEEE Trans. Magn. **31**, 3793 (1995); R. O'Barr, M. Lederman, S. Schultz, W. Xu, A. Scherer, and J. Tonucci, J. Appl. Phys. **79**, 5303 (1996).

[14] A. Aharoni and S. Shtrikman, Phys. Rev. **109**, 1522 (1958); E. H. Frei, S. Shtrikman, and D. Treves, *ibid.* **106**, 446 (1957), and references therein.

[15] J. L. Maurice, D. Imhoff, P. Etienne, O. Durand, S. Dubois, L. Piraux, J. M. George, P. Galtier, and A. Fert (unpublished).

[16] E. Ferain and R. Legras, Nucl. Instrum. Methods Phys. Res. (to be published).

[17] L. Piraux, S. Dubois, E. Ferain, R. Legras, K. Ounadjela, J. M. George, J. L. Maurice, and A. Fert, J. Magn. Magn. Mater. **165**, 352 (1997).

[18] W. Wernsdorfer (private communication).

[19] E. Koerster and T. C. Arnoldussen, in *Magnetic Recording*, edited by C. D. Mee and E. D. Daniel (McGraw-Hill, New York, 1987), Vol. 1.

[20] P. Lefebvre (private communication).

[21] E. C. Stoner and E. P. Wolfarth, Philos. Trans. R. Soc. London, Ser. A **240**, 599 (1948).

[22] I. S. Jacobs and F. E. Luborsky, J. Appl. Phys. **28**, 467 (1957).

[23] T. R. McGuire and R. I. Potter, IEEE Trans. Magn. **11**, 1018 (1975); for a review, see I. A. Campbell and A. Fert, in *Transport Properties of Ferromagnets*, edited by E. P. Wohlfarth (North-Holland, Amsterdam, 1982), Vol. 3, Chap. 9.

[24] R. Ferré, Comput. Phys. Commun. (to be published).

[25] A. Aharoni, Phys. Rev. **131**, 1478 (1963).

[26] All the explored cases reveal differences not exceeding 5% in nucleation field values between cylinders and square prisms; R. Ferré, Comp. Mater. Sci. (to be published); for results comparing the nucleation fields in infinite rectangular bars and in infinite cylinders see W. F. Brown, Jr., J. Appl. Phys. **33**, 3026 (1962); A. Aharoni, Phys. Status Solidi **16**, 3 (1966).

[27] Y. D. Yang and E. Della Torre, J. Appl. Phys. **66**, 320 (1989).

[28] Y. D. Yang and E. Della Torre, IEEE Trans. Magn. **24**, 2368 (1988); R. Ferré, Ph.D. thesis, Univ. Joseph Fourier, Grenoble (1995).

[29] A. Hubert, *Theorie der Domänenwände in Geordneten Medien* (Springer, Berlin, 1974); J. Miltat, in *Applied Magnetism*, Vol. 253 of *NATO Advanced Study Institute, Series E: Applied Sciences*, edited by R. Guber, C. B. Wright, and G. Arti (Kluwer, New York, 1994).

[30] I. M. Croll, IEEE Trans. Magn. **MAG-23**, 59 (1987); H. Daimon and O. Kitakami, J. Appl. Phys. **73**, 5391 (1993).

[31] S. T. Roschenko, I. G. Shipkova, B. M. Baizuldin, K. N. Gavrilenko, and E. V. Panasenko, J. Magn. Magn. Mater. **148**, 108 (1995).